025921-10-T

THE UNIVERSITY OF MICHIGAN

COLLEGE OF ENGINEERING

DEPARTMENT OF ELECTRICAL ENGINEERING & COMPUTER SCIENCE

Radiation Laboratory

A NEW TECHNIQUE FOR SIMULATING COMPOSITE MATERIAL
Task 1: A Finite Element Conjugate Gradient FFT Method for Scattering

Report Title: A Finite Element-Boundary Integral Formualtion For Scattering by Three-Dimensional Cavity-Backed Apertures

Jian-Ming Jin and John L. Volakis
Radiation Laboratory
Department of Electrical Engineering
and Computer Science
The University of Michigan
Ann Arbor, MI 48109

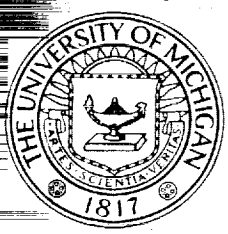

September 1989 - February 1990

NAG2-541

Ann Arbor, Michigan

TECHNICAL REPORT

FOR

NASA Grant NAG-2-541

NASA Technical Monitor: Alex Woo

Grant Title: A NEW TECHNIQUE FOR SIMULATING COMPOSITE MATERIAL
Task 1: A Finite Element Conjugate Gradient FFT Method for Scattering

Institution: The Radiation Laboratory
Department of Electrical Engineering and Computer Science
The University of Michigan
Ann Arbor, MI 48109-2122

Period Covered: September 1989 - February 1990

Report Title: A Finite Element-Boundary Integral Formulation For Scattering by Three-Dimensional Cavity-Backed Apertures

Report Authors: Jian-Ming Jin and John L. Volakis

Principal Investigator: John L. Volakis
Telephone: (313) 764-0500

A FINITE ELEMENT-BOUNDARY INTEGRAL FORMULATION FOR SCATTERING BY THREE-DIMENSIONAL CAVITY-BACKED APERTURES

Jian-Ming Jin and John L. Volakis

Radiation Laboratory

Department of Electrical Engineering and Computer Science

The University of Michigan

Ann Arbor, Michigan 48109

ABSTRACT

A new numerical technique is proposed for the electromagnetic characterization of the scattering by a three-dimensional cavity-backed aperture in an infinite ground plane. The technique combines the finite element and boundary integral methods to formulate a system of equations for the solution of the aperture fields and those inside the cavity. Specifically, the finite element method is employed to formulate the fields in the cavity region and the boundary integral approach is used in conjunction with the equivalence principle to represent the fields above the ground plane. Unlike traditional approaches, the proposed technique does not require knowledge of the cavity's Green's function and is, therefore, applicable to arbitrary shape depressions and material fillings. Furthermore, the proposed formulation leads to a system having a partly full and partly sparse as well as symmetric and banded matrix which can be solved efficiently using special algorithms.

I. INTRODUCTION

Recently, a new technique which combines the finite element and boundary integral formulations to yield a system for solution via the conjugate gradient method (CGM) and the fast Fourier transform (FFT) was proposed for electromagnetic scattering computations. In particular, the method was formulated for the characterization of filled slots and grooves in a thick ground plane with transverse electric (TE) and transverse magnetic (TM) incidence [1], [2]. A similar technique was also proposed in [3] for computing the aperture admittance matrix of the same geometry, but in that procedure a frontal solution algorithm was employed to reduce the memory demand. In this paper we describe an extension of the hybrid technique proposed in [1], [2] for the electromagnetic characterization of three-dimensional (3-D) cavity-backed apertures in a ground plane.

The problem of scattering by 3-D cavity-backed apertures in a ground plane has been considered in the past via the mode matching [4] and moment method/modal [5] approaches. A unique feature of both of these techniques is a required knowledge of the cavity's Green's function. They are, thus, mostly restricted to rectangular cavities, but even then, additional difficulties may arise. For example, the mode matching technique yields an infinite matrix that must be truncated and in the case of the moment method/modal approach the admittance elements involve mode sums that are usually slowly converging. Neither of these methodologies are obviously capable of treating large size apertures but in the case of deep cavities, high frequency techniques such as those proposed in [6] and [7] could be effectively employed. Nevertheless, when the cavity is narrow in one dimension or shallow and perhaps filled with inhomogeneous material, a numerical solution approach is the likely alternative.

A numerical approach which has demonstrated promise for treating large structures is the finite difference-time domain approach (FD-TD) [8]. In this case the finite difference mesh must be terminated with an absorbing boundary condition. In contrast, the proposed approach avoids possible truncation errors and excess discretization by representing the fields external to the cavity with the appropriate boundary integrals. Specifically, the proposed approach employs the finite element method [9] to formulate the fields within the cavity whereas the fields external to the cavity are expressed via the radiation integrals over the aperture. The resulting equations are then solved by demanding continuity of the tangential fields across the aperture. By virtue of the finite element method, the technique is applicable to cavities of arbitrary shape, possibly filled with inhomogeneous or composite materials. In the following sections the proposed hybrid formulation is discussed in some detail along with the pertinent discretization of the resulting integral equations. A number of results are then presented which validate the formulation and we conclude with a discussion on the method's merits and possible improvements.

II. FORMULATION

Consider the 3-D cavity-backed aperture illustrated in Figure 1. We will denote the free space region above the cavity ($z > 0$) as region I and that inside the cavity ($-c < z < 0$) as region II occupying the volume V. We will further assume that the cavity is filled with an inhomogeneous material having a relative permittivity $\epsilon_r(\mathbf{R})$ and relative permeability $\mu_r(\mathbf{R})$.

In accordance with the equivalence principle [10], the fields in the two regions can be

decoupled by closing the aperture with a perfect conductor and introducing the equivalent magnetic current

$$\mathbf{M} = \mathbf{E} \times \hat{\mathbf{z}} \tag{1}$$

over the extent of the aperture, where $\mathbf{E}$ is the electric field at the aperture ($z = 0$). The field in region I is then due to the radiation caused by the equivalent current $\mathbf{M}$ residing on the ground plane and possibly by other impressed sources ($\mathbf{J}^i$, $\mathbf{M}^i$). Accordingly, by invoking image theory we have

$$\mathbf{H}^I(\mathbf{R}) = \mathbf{H}^i(\mathbf{R}) + \mathbf{H}^r(\mathbf{R}) - 2jk_0Y_0 \iint_S \bar{\bar{\mathbf{G}}}_0(\mathbf{R}, \mathbf{R}') \bullet \mathbf{M}(\mathbf{R}')dS' \tag{2}$$

where $\mathbf{H}^i$ denotes the incident field due to ($\mathbf{J}^i$, $\mathbf{M}^i$) and $\mathbf{H}^r$ is that reflected by the ground plane without the aperture. Also, $k_0 = 2\pi/\lambda$ is the free space wavenumber, $Z_0 = 1/Y_0$ is the free space intrinsic impedance, S denotes the planar surface area of the aperture and $\bar{\bar{\mathbf{G}}}_0$ is the free-space dyadic Green's function given by

$$\bar{\bar{\mathbf{G}}}_0(\mathbf{R}, \mathbf{R}') = \left(\bar{\bar{\mathbf{I}}} + \frac{1}{k_0^2}\nabla\nabla\right) G_0(\mathbf{R}, \mathbf{R}') \tag{3}$$

with

$$\bar{\bar{\mathbf{I}}} = \hat{\mathbf{x}}\hat{\mathbf{x}} + \hat{\mathbf{y}}\hat{\mathbf{y}} + \hat{\mathbf{z}}\hat{\mathbf{z}} \quad \text{and} \quad G_0(\mathbf{R}, \mathbf{R}') = \frac{e^{-jk_0|\mathbf{R}-\mathbf{R}'|}}{4\pi|\mathbf{R} - \mathbf{R}'|}.$$

Enforcing continuity of the tangential electric fields across the aperture, we find that the field in region II can be represented by the radiation of the equivalent magnetic current $-\mathbf{M}$. The fields in the two regions are then coupled by enforcing continuity of the tangential magnetic fields across the aperture. This gives

$$\hat{\mathbf{z}} \times \mathbf{H}^I(\mathbf{M}, \mathbf{J}^i, \mathbf{M}^i) = \hat{\mathbf{z}} \times \mathbf{H}^{II}(-\mathbf{M}) \quad \text{at } z = 0 \tag{4}$$

where $\mathbf{H}^I$ and $\mathbf{H}^{II}$ denote the magnetic fields in regions I and II, respectively.

Traditionally, $\mathbf{M}$ is solved from (4) by substituting for $\mathbf{H}^I$ as given in (2) and expressing $\mathbf{H}^{II}$ as a function/integral of $\mathbf{M}$. The resulting integral equation(s) are then discretized to obtain a system of equations for solution via direct inversion or LU decomposition. However, to explicitly express $\mathbf{H}^{II}$ in terms of $\mathbf{M}$ implies a knowledge of the cavity's Green's function. For rectangular cavities filled with homogeneous material, this is usually found in modal form which is in general computationally inefficient [5]. Furthermore, in the case of arbitrarily shaped and/or inhomogeneously filled cavities there is no available closed form of the associated Green's function. As a result, so far numerical solutions have only been considered for cavities that are rectangular and filled with homogeneous or uniformly layered material [4], [5].

To overcome the difficulty associated with the availability of the cavity Green's function, we employ the finite element method to formulate the fields in the cavity region (region II). Specifically, the cavity fields are demanded to satisfy the variational equation

$$\delta F = 0 \tag{5}$$

where the functional F is given by [11]

$$\begin{aligned} F\left(\mathbf{E}^{II}\right) &= \frac{1}{2}\iiint_V \left[\frac{1}{\mu_r}\left(\nabla\times\mathbf{E}^{II}\right)\bullet\left(\nabla\times\mathbf{E}^{II}\right)+\frac{s}{\mu_r\epsilon_r^2}\left(\nabla\bullet\epsilon_r\mathbf{E}^{II}\right)^2\right. \\ &\quad \left.-k_0^2\epsilon_r\mathbf{E}^{II}\bullet\mathbf{E}^{II}\right]dV + jk_0Z_0\oiint_{S_{cav}}\left(\mathbf{E}^{II}\times\mathbf{H}^{II}\right)\bullet\hat{\mathbf{n}}dS \end{aligned} \tag{6}$$

if the variation is taken with respect to the electric field or by

$$\begin{aligned} F\left(\mathbf{H}^{II}\right) &= \frac{1}{2}\iiint_V \left[\frac{1}{\epsilon_r}\left(\nabla\times\mathbf{H}^{II}\right)\bullet\left(\nabla\times\mathbf{H}^{II}\right)+\frac{s}{\epsilon_r\mu_r^2}\left(\nabla\bullet\mu_r\mathbf{H}^{II}\right)^2\right. \\ &\quad \left.-k_0^2\mu_r\mathbf{H}^{II}\bullet\mathbf{H}^{II}\right]dV + jk_0Y_0\oiint_{S_{cav}}\left(\mathbf{E}^{II}\times\mathbf{H}^{II}\right)\bullet\hat{\mathbf{n}}dS \end{aligned} \tag{7}$$

if the variation is taken with respect to the magnetic field. In these, V denotes the volume occupied by region II, S_{cav} corresponds to the surface that encloses V and $\hat{\mathbf{n}}$ denotes the unit vector normal to the surface, pointing away from the cavity. Since the divergence of $\mathbf{E}^{II}$ is zero in the source free region, it would appear that the second term in (6) and (7) is superfluous and, in fact, it is not included in the corresponding expressions found in [11]. However, a solution of (5) with $s = 0$ does not guarantee that the resulting fields will be maxwellian unless the divergence conditions are also satisfied. In the case of two-dimensional solutions they are satisfied *a priori* but not so for three-dimensional implementations. Here we propose that the divergence conditions be satisfied approximately and implicitly [12] by minimizing (6) or (7) with $s \neq 0$. The parameter s is referred to as the penalty factor and its choice will be discussed later.

To solve (6) or (7), it is necessary that the fields be known over the surface specified by S_{cav}. Obviously, the boundary conditions to be imposed on the conducting boundaries of the cavity are

$$\hat{\mathbf{n}} \times \mathbf{E}^{II} = 0 \tag{8}$$

and

$$\hat{\mathbf{n}} \bullet \mathbf{H}^{II} = 0. \tag{9}$$

Substituting these into (6) and (7) eliminates the portion of the surface integral over the conducting boundary of the cavity (that is, there is no power flow through the metallic portion of S_{cav}). It remains to specify the boundary condition over the cavity's aperture and this is given by (1). With these boundary conditions we may proceed with

a discretization of (5) which in conjunction with the discretization of (2) yields a system for a solution of $\mathbf{M}$. Here the continuity condition (4) is enforced upon the discretized fields and this is the standard procedure employed in general finite element-boundary integral formulation [13]. However, if (6) is used the enforcement of (4) can be executed at the analytical stage by substituting (2) into (6). Doing so, we obtain the functional

$$\begin{aligned} F &= \frac{1}{2}\iiint_V \left[\frac{1}{\mu_r}\left(\nabla\times\mathbf{E}^{II}\right)\bullet\left(\nabla\times\mathbf{E}^{II}\right)+\frac{s}{\mu_r\epsilon_r^2}\left(\nabla\bullet\epsilon_r\mathbf{E}^{II}\right)^2-k_0^2\epsilon_r\mathbf{E}^{II}\bullet\mathbf{E}^{II}\right]dV \\ &\quad -2k_0^2\iint_S \mathbf{M}(\mathbf{R})\bullet\left[\iint_S \bar{\bar{\mathrm{G}}}_0(\mathbf{R},\mathbf{R}')\bullet\mathbf{M}(\mathbf{R}')dS'\right]dS \\ &\quad -jk_0Z_0\iint_S \mathbf{M}(\mathbf{R})\bullet\left[\mathbf{H}^i(\mathbf{R})+\mathbf{H}^r(\mathbf{R})\right]dS \end{aligned} \tag{10}$$

which can be discretized via the finite element method for a solution of $\mathbf{M}$. Once $\mathbf{M}$ is found, the far zone scattered field can be easily computed from

$$\mathbf{H}^s(\mathbf{R}) = -jk_0Y_0\frac{e^{-jk_0R}}{2\pi R}\iint_S(\hat{\theta}\hat{\theta}+\hat{\phi}\hat{\phi})\bullet\mathbf{M}(x',y')e^{jk_0\sin\theta(x'\cos\phi+y'\sin\phi)}dx'dy' \tag{11}$$

where (R,θ,ϕ) are the usual spherical coordinates of the observation point. The radar cross section (RCS) of the aperture is then given by

$$\sigma = \lim_{R\to\infty} 4\pi R^2\frac{|\mathbf{H}^s(\mathbf{R})|^2}{|\mathbf{H}^i(\mathbf{R})|^2}. \tag{12}$$

III. FINITE ELEMENT DISCRETIZATION

For a numerical implementation of (5) we must first discretize the functionals by subdividing V and S into smaller volume and surface elements, respectively. Considering the electric field formulation, it is convenient to rewrite the functional F as

$$F = F_V + F_S + F_E \tag{13}$$

where F_V is the volume integral

$$F_V = \frac{1}{2}\iiint_V \left\{ \frac{1}{\mu_r}\left[\left(\frac{\partial E_z}{\partial y} - \frac{\partial E_y}{\partial z}\right)^2 + \left(\frac{\partial E_x}{\partial z} - \frac{\partial E_z}{\partial x}\right)^2 + \left(\frac{\partial E_y}{\partial x} - \frac{\partial E_x}{\partial y}\right)^2\right] + \frac{s}{\mu_r \epsilon_r^2}\left[\frac{\partial(\epsilon_r E_x)}{\partial x} + \frac{\partial(\epsilon_r E_y)}{\partial y} + \frac{\partial(\epsilon_r E_z)}{\partial z}\right]^2 - k_0^2 \epsilon_r \left(E_x^2 + E_y^2 + E_z^2\right)\right\} dV \qquad (14)$$

obtained by expanding the appropriate integrand in (10) and F_S denotes the surface integral

$$F_S = -2k_0^2 \iint_S \mathbf{M}(\mathbf{R}) \bullet \left[\iint_S \bar{\bar{\mathrm{G}}}_0(\mathbf{R}, \mathbf{R}') \bullet \mathbf{M}(\mathbf{R}') dS'\right] dS. \qquad (15)$$

The remaining portion of F is associated with the source field and is given by

$$F_E = -2jk_0 Z_0 \iint_S \mathbf{M}(\mathbf{R}) \bullet \mathbf{H}^i(\mathbf{R}) dS \qquad (16)$$

upon using the relation $\hat{\mathbf{z}} \times \mathbf{H}^r(\mathbf{R}) = \hat{\mathbf{z}} \times \mathbf{H}^i(\mathbf{R})$. For simplicity, in (14) we have omitted the superscript II and this practice will be continued in the remaining portion of the paper.

To discretize (14) we subdivide the volume V into M_v small volume elements such as tetrahedra, triangular prisms, or rectangular bricks. Within the eth element having n nodes, the field components are expressed as

$$E_p = \sum_{j=1}^{n} N_j^e(x, y, z)\phi_{pj}^e \qquad p = x, y, z \qquad (17)$$

where N_j^e are the known expansion or shape functions (see Appendix) chosen so that ϕ_{pj}^e $(p = x, y, z)$ represents the unknown field at the jth node of the eth element. Substituting (17) into (14) yields the portion of F_V attributed to the eth element. The complete expression for F_V is then obtained by summing/assembling the contributions from all

elements. This yields a functional in terms of the unknown node field components which must be found to satisfy (5). In accordance with the Rayleigh-Ritz procedure this is equivalent to setting the derivatives of F with respect to the node fields ϕ^e_{pj} $(p = x, y, z)$ equal to zero. Differentiating the portion of F_V attributed to the eth element with respect to the node field ϕ^e_{xi} we obtain

$$\begin{aligned}\frac{\partial F^e_V}{\partial \phi^e_{xi}} &= \sum_{j=1}^{n} \iiint_{V^e} \frac{1}{\mu_r} \left\{ \left[\frac{s}{\epsilon_r^2} \frac{\partial(\epsilon_r N^e_i)}{\partial x} \frac{\partial(\epsilon_r N^e_j)}{\partial x} + \frac{\partial N^e_i}{\partial y}\frac{\partial N^e_j}{\partial y} + \frac{\partial N^e_i}{\partial z}\frac{\partial N^e_j}{\partial z} \right.\right. \\ &\quad \left. - k_0^2 \epsilon_r \mu_r N^e_i N^e_j \right] \phi^e_{xj} + \left[\frac{s}{\epsilon_r^2} \frac{\partial(\epsilon_r N^e_i)}{\partial x} \frac{\partial(\epsilon_r N^e_j)}{\partial y} - \frac{\partial N^e_i}{\partial y}\frac{\partial N^e_j}{\partial x} \right] \phi^e_{yj} \\ &\quad \left. + \left[\frac{s}{\epsilon_r^2} \frac{\partial(\epsilon_r N^e_i)}{\partial x} \frac{\partial(\epsilon_r N^e_j)}{\partial z} - \frac{\partial N^e_i}{\partial z}\frac{\partial N^e_j}{\partial x} \right] \phi^e_{zj} \right\} dV. \end{aligned} \tag{18}$$

Similarly, by differentiating with respect to the other node field components we have

$$\begin{aligned}\frac{\partial F^e_V}{\partial \phi^e_{yi}} &= \sum_{j=1}^{n} \iiint_{V^e} \frac{1}{\mu_r} \left\{ \left[\frac{s}{\epsilon_r^2} \frac{\partial(\epsilon_r N^e_i)}{\partial y} \frac{\partial(\epsilon_r N^e_j)}{\partial x} - \frac{\partial N^e_i}{\partial x}\frac{\partial N^e_j}{\partial y} \right] \phi^e_{xj} \right. \\ &\quad + \left[\frac{\partial N^e_i}{\partial x}\frac{\partial N^e_j}{\partial x} + \frac{s}{\epsilon_r^2} \frac{\partial(\epsilon_r N^e_i)}{\partial y} \frac{\partial(\epsilon_r N^e_j)}{\partial y} + \frac{\partial N^e_i}{\partial z}\frac{\partial N^e_j}{\partial z} - k_0^2 \epsilon_r \mu_r N^e_i N^e_j \right] \phi^e_{yj} \\ &\quad \left. + \left[\frac{s}{\epsilon_r^2} \frac{\partial(\epsilon_r N^e_i)}{\partial y} \frac{\partial(\epsilon_r N^e_j)}{\partial z} - \frac{\partial N^e_i}{\partial z}\frac{\partial N^e_j}{\partial y} \right] \phi^e_{zj} \right\} dV \end{aligned} \tag{19}$$

and

$$\begin{aligned}\frac{\partial F^e_V}{\partial \phi^e_{zi}} &= \sum_{j=1}^{n} \iiint_{V^e} \frac{1}{\mu_r} \left\{ \left[\frac{s}{\epsilon_r^2} \frac{\partial(\epsilon_r N^e_i)}{\partial z} \frac{\partial(\epsilon_r N^e_j)}{\partial x} - \frac{\partial N^e_i}{\partial x}\frac{\partial N^e_j}{\partial z} \right] \phi^e_{xj} \right. \\ &\quad + \left[\frac{s}{\epsilon_r^2} \frac{\partial(\epsilon_r N^e_i)}{\partial z} \frac{\partial(\epsilon_r N^e_j)}{\partial y} - \frac{\partial N^e_i}{\partial y}\frac{\partial N^e_j}{\partial z} \right] \phi^e_{yj} + \left[\frac{\partial N^e_i}{\partial x}\frac{\partial N^e_j}{\partial x} \right. \\ &\quad \left. \left. + \frac{\partial N^e_i}{\partial y}\frac{\partial N^e_j}{\partial y} + \frac{s}{\epsilon_r^2} \frac{\partial(\epsilon_r N^e_i)}{\partial z} \frac{\partial(\epsilon_r N^e_j)}{\partial z} - k_0^2 \epsilon_r \mu_r N^e_i N^e_j \right] \phi^e_{zj} \right\} dV. \end{aligned} \tag{20}$$

We observe that if ϵ_r and μ_r are assumed constant within the eth element, all integrals in (18)-(20) can be evaluated analytically. Otherwise, a numerical integration may be be required for their evaluation.

Let us now consider the discretization of the surface integral in (15). A difficulty in the evaluation of this integral is the usual singularity associated with the derivatives of the free space Green's function. This, however, can be avoided by transfering the derivatives to the current. To do so, we invoke a common vector identity and the divergence theorem, leading to

$$\begin{aligned} F_S &= -2\iint_S \mathbf{M}(\mathbf{R}) \bullet \Big[k_0^2 \iint_S \mathbf{M}(\mathbf{R}')G_0(\mathbf{R},\mathbf{R}')dS' \\ &\qquad +\nabla \iint_S \nabla' \bullet \mathbf{M}(\mathbf{R}')G_0(\mathbf{R},\mathbf{R}')dS'\Big]\, dS. \end{aligned} \tag{21}$$

Through the same process, (21) can be further rewritten as

$$\begin{aligned} F_S &= -2k_0^2 \iint_S \mathbf{M}(\mathbf{R}) \bullet \Big[\iint_S \mathbf{M}(\mathbf{R}')G_0(\mathbf{R},\mathbf{R}')dS'\Big]\, dS \\ &\qquad +2\iint_S \nabla \bullet \mathbf{M}(\mathbf{R}) \Big[\iint_S \nabla' \bullet \mathbf{M}(\mathbf{R}')G_0(\mathbf{R},\mathbf{R}')dS'\Big]\, dS \end{aligned} \tag{22}$$

and by invoking (1) we obtain

$$\begin{aligned} F_S &= -2k_0^2 \iint_S E_x \Big[\iint_S E_x G_0 dS'\Big]\, dS + 2k_0^2 \iint_S E_y \Big[\iint_S E_y G_0 dS'\Big]\, dS \\ &\qquad +2\iint_S \Big(\frac{\partial E_x}{\partial y} - \frac{\partial E_y}{\partial x}\Big) \Big[\iint_S \Big(\frac{\partial E_x}{\partial y'} - \frac{\partial E_y}{\partial x'}\Big) G_0 dS'\Big]\, dS \end{aligned} \tag{23}$$

which can be discretized by subdividing S into M_s smaller surface elements. In parallel with the volume discretization, the field components in the eth surface element can be expressed as

$$E_p = \sum_{j=1}^{n_s} N_j^e(x,y)\phi_{pj}^e \qquad p = x, y \tag{24}$$

where n_s denotes the number of nodes associated with the area element, N_j^e are the same expansion functions as those in (17) with $z = 0$ and ϕ_{pj}^e $(p = x, y)$ represent the

node fields. Substituting (24) into (23) and replacing S in the first pair of integrals with S^e, the area of the eth surface element, gives the portion of F_S attributed to the eth element. As noted earlier, to enforce the stationarity condition we need the derivatives of F_S with respect to the node fields. For the eth element we have

$$\begin{aligned}\frac{\partial F_S^e}{\partial \phi_{xi}^e} &= -2k_0^2 \iint_{S^e} N_i^e \left[\sum_{e=1}^{M_s} \sum_{j=1}^{n_s} \phi_{xj}^e \iint_{S^e} N_j^e G_0 dS' \right] dS \\ &\quad +2 \iint_{S^e} \frac{\partial N_i^e}{\partial y} \left[\sum_{e=1}^{M_s} \sum_{j=1}^{n_s} \iint_{S^e} \left(\frac{\partial N_j^e}{\partial y'} \phi_{xj}^e - \frac{\partial N_j^e}{\partial x'} \phi_{yj}^e \right) G_0 dS' \right] dS, \qquad (25)\end{aligned}$$

$$\begin{aligned}\frac{\partial F_S^e}{\partial \phi_{yi}^e} &= -2k_0^2 \iint_{S^e} N_i^e \left[\sum_{e=1}^{M_s} \sum_{j=1}^{n_s} \phi_{yj}^e \iint_{S^e} N_j^e G_0 dS' \right] dS \\ &\quad -2 \iint_{S^e} \frac{\partial N_i^e}{\partial x} \left[\sum_{e=1}^{M_s} \sum_{j=1}^{n_s} \iint_{S^e} \left(\frac{\partial N_j^e}{\partial y'} \phi_{xj}^e - \frac{\partial N_j^e}{\partial x'} \phi_{yj}^e \right) G_0 dS' \right] dS \qquad (26)\end{aligned}$$

and $\partial F_S^e / \partial \phi_{zi}^e = 0$ since F_S is not a function of E_z. We note that in deriving (25) and (26) the differentiation was performed only with respect to the node fields outside the square brackets in (23) while those introduced by substituting (2) into (6) remained uneffected. Further, we remark that the evaluation of the surface integrals in (25) and (26), although not trivial, can be done through analytical and numerical means as discussed in the Appendix.

It remains to discretize (16) which involves the excitation fields. By replacing M with E in accordance with (1) we obtain

$$F_E = 2jk_0 Z_0 \iint_S \left(E_x H_y^i - E_y H_x^i \right) dS. \qquad (27)$$

This can again be discretized by introducing the expansion (24) and by doing so we

obtain (for the eth element only)

$$\frac{\partial F_E^e}{\partial \phi_{xi}^e} = 2jk_0 Z_0 \iint_{S^e} N_i^e H_y^i dS \tag{28}$$

and

$$\frac{\partial F_E^e}{\partial \phi_{yi}^e} = -2jk_0 Z_0 \iint_{S^e} N_i^e H_x^i dS \tag{29}$$

Given the partial derivatives of all integral functions comprising the functional F we can now proceed with the construction of the final system of equations by imposing the stationarity condition (5). This implies that

$$\begin{aligned}
\frac{\partial F}{\partial \phi_{xi}} &= \sum_{e=1}^{M_v} \frac{\partial F_V^e}{\partial \phi_{xi}^e} + \sum_{e=1}^{M_s} \frac{\partial F_S^e}{\partial \phi_{xi}^e} + \sum_{e=1}^{M_s} \frac{\partial F_E^e}{\partial \phi_{xi}^e} = 0 \\
\frac{\partial F}{\partial \phi_{yi}} &= \sum_{e=1}^{M_v} \frac{\partial F_V^e}{\partial \phi_{yi}^e} + \sum_{e=1}^{M_s} \frac{\partial F_S^e}{\partial \phi_{yi}^e} + \sum_{e=1}^{M_s} \frac{\partial F_E^e}{\partial \phi_{yi}^e} = 0 \\
\frac{\partial F}{\partial \phi_{zi}} &= \sum_{e=1}^{M_v} \frac{\partial F_V^e}{\partial \phi_{zi}^e} = 0 \qquad\qquad i = 1, 2, 3, ..., N
\end{aligned} \tag{30}$$

leading to a matrix system for the solution of the node fields. In (30) N denotes the total number of nodes, ϕ_{pi} $(p = x, y, z)$ are the node fields labeled with global indices and as before ϕ_{pi}^e $(p = x, y, z)$ are the node fields associated with the eth volume or surface element. Both ϕ_{pi} and ϕ_{pi}^e refer to the field at the same node and thus the eth term of the summations have non-zero values only if the global node i belong to the eth element. The system implied by (30) must, of course, be solved after imposing the boundary condition (8) which permits us to zero out those field components that belong to nodes on metallic boundaries and are also tangential to that boundary. This reduces substantially the number of unknowns in the system which can then be solved via direct inversion, LU decomposition, or iteration. However, since the system matrix is partly full

and partly sparse as well as symmetric and banded (if the nodes are properly numbered), it can be more efficiently solved by those algorithms which exploit these properties [14]. Various partition techniques such as the those discussed in [15] can also be employed to enhance the efficiency of the solution. Further, the matrix system is amenable to a conjugate gradient-fast Fourier transform solution, thus, reducing the memory demand to O(N) as in [1], [2].

Let us now briefly address the formulation resulting from a finite element discretization of (7). In this case we cannot invoke (4) to incorporate (2) into (7) and obtain an expression that is completely in terms of the unknown nodal magnetic fields. As a result, the continuity condition (4) must be explicitly imposed leading to a second system of equations to be coupled with that from the discretization of (7). The penalty with this approach is an increase in the number of unknowns because the surface magnetic currents or electric fields must be added to the nodal magnetic fields resulting from the discretization of region II. Accordingly, the system resulting from (7) is of the form

$$[K]\{\phi\} + [B]\{\psi_S\} = 0 \tag{31}$$

where $\{\phi\}$ is a column vector representing the nodal values of the discretized magnetic field in the cavity and over the aperture, and $\{\psi_S\}$ is a similar column for the discretized aperture electric fields. The matrix $[K]$ is square and symmetric whereas $[B]$ is rectangular. Further, both matrices are very sparse and banded provided the nodes are properly numbered. A corresponding discretization of (2) via Galerkin's methods leads to

$$[B]^T\{\phi\} + [P]\{\psi_S\} = \{b\} \tag{32}$$

where the superscript T denote the transpose and $[P]$ is a full, square and symmetric

matrix. Further, $\{b\}$ is the excitation column vector and is a function of the incident field. Combining (31) and (32) yields a symmetric system that can be solved after imposing the boundary condition (9).

IV. NUMERICAL RESULTS

We present in this section some results for reference purposes and for validating the proposed formulation. In all cases, the excitation is a plane wave given by

$$\mathbf{E}^i(\mathbf{R}) = [(\hat{\alpha} \bullet \hat{\theta}^i)\hat{\theta}^i + (\hat{\alpha} \bullet \hat{\phi}^i)\hat{\phi}^i]e^{-j\mathbf{k}^i \bullet \mathbf{R}} \tag{33}$$

where $\hat{\alpha} = \hat{\theta}^i \cos\alpha + \hat{\phi}^i \sin\alpha$ is the polarization vector, $\mathbf{k}^i$ is the propagation vector given by

$$\mathbf{k}^i = -k_0(\sin\theta^i \cos\phi^i \hat{\mathbf{x}} + \sin\theta^i \sin\phi^i \hat{\mathbf{y}} + \cos\theta^i \hat{\mathbf{z}}) \tag{34}$$

and $\hat{\theta}^i$ and $\hat{\phi}^i$ are the usual unit vectors in the spherical system and are associated with the angles θ^i and ϕ^i. Further, in all computations the penalty factor s was set to unity and rectangular bricks were used for the discretization of region II.

For reference, Figure 2 shows the y-component of the electric field along the center of an aperture formed by a narrow crack of length $a = 0.5\lambda$, 1.0λ, 1.5λ and 2.0λ. We remark that the behavior of the aperture field associated with the cavity-backed structure is distinctly different from that of a transmitting aperture as given in [16].

Figure 3 displays the co-polarized and cross-polarized backscatter RCS of a deep empty cavity as compared with data obtained via the moment method/modal approach [5]. Overall the agreement between the results from the two methods is seen to be excellent except at the point ($\phi = 90°$) for $\alpha = 90°$. We also note that the data in

this figure are in agreement with those obtained using the mode matching procedure [4]. For the same aperture size, Figure 4 displays the cavity RCS as a function of depth. The resonant behavior of the cavity is rather distinct and characteristic of the cavity dimensions.

The backscatter RCS of a material filled cavity is displayed in Figure 5. The results based on this formulation and the moment method/modal approach are again in excellent agreement. Finally, Figure 6 refers to a cavity filled with multilayer material. The presented formulation is, of course, applicable to cavities filled with inhomogeneous material whereas traditional approaches are not. Further, arbitrary shape cavities can be treated with the same ease by employing an appropriate mesh generation algorithm.

V. DISCUSSION

There are a few issues which must be addressed in connection with the proposed formulation and the solution of the resulting system. In particular, below we discuss the role and choice of the penalty factor and the difficulty associated with the representation of the fields near corners and edges. Also, a few remarks are included with respect to the efficiency of this solution versus those based on more traditional approaches.

A. Penalty Term

As we stated above, the role of the penalty term is to implicitly satisfy the divergence conditions on the electric and magnetic fields. The term was first introduced in the stationary functional to remove the spurious modes that often appear in finite element solutions of eigenvalue problems such as those pertaining to waveguides and closed cavities [12]. For those problems the role of the penalty term was very crucial in determining

the proper modes, propagation constant or resonant frequencies. For this application we observed that in most cases the actual value of the penalty factor (s from 0 to 2) has a small effect on the RCS pattern. Nevetheless, it is desirable to avoid the ambiguity associated with the penalty term and this can be accomplished by using divergenceless basis functions [17].

B. Corner/Edge Conditions

It is known [18] that some field components are singular near sharp perfectly conducting edges as is the case with the four edges forming the aperture in Figure 1. The basis functions used in this paper or other similar conventional basis functions are not capable of accurately representing those field singularities. This, of course, leads to errors in the calculated field distribution which can be avoided by modifying the field expansion to include basis functions that simulate its expected singular behavior as determined from a static solution. A successful example of this is given in [19] and the approach could be extended to three-dimensions. We note that for the computations in this paper we did not observe a noticeable effect on the RCS pattern due to errors associated with the edge condition.

C. Computational Efficiency

The proposed formulation was considered because of its potential to treat cavities of arbitrary shape and material fillings. However, it was also found more computationally efficient than tradiational formulations [4], [5] without even making use of the symmetry and sparseness properties of the resulting matrix. In particular, by using LU decomposition for the solution of the matrix system, the data in Figure 3 were generated in less than one minute on an Apollo DN10000. In contrast, the corresponding time when

using the mode matching technique was five minutes on a Cray XMP-48 [4] and that for the moment method/modal approach was two minutes on an Apollo DN10000. The CPU time differences between the moment method/modal approach and the proposed formulation are even more apart for larger apertures. For example, the data in Figure 5 were obtained in four minutes on an Apollo DN10000 by this method but 65 minutes were required with the moment method/modal approach on the same machine. A major reason for the large difference in CPU time is due to the slowly converging mode sums that must be evaluated in the process of generating the matrix elements.

VI. SUMMARY

A new technique was proposed for a numerical characterization of the scattering by a 3-D cavity-backed aperture in a ground plane. The proposed technique combines the finite element and boundary integral methods to generate a system of equations for the aperture fields in conjunction with the continuity condition at the aperture. In principle, the technique is capable of treating arbitrarily shaped cavities filled with inhomogeneous materials. However, because of the lack of available reference data, the proposed solution was only validated for rectangular cavities. Some important issues relating to the implementation and effciency of the technique were also discussed.

APPENDIX

A suitable element for the discretization of a rectangular cavity is the rectangular brick illustrated in Figure 7. For this element, the expansion functions in (17) are given by

$$N_1^e = \frac{(a'-x')(b'-y')(c'-z')}{a'b'c'} \quad N_2^e = \frac{x'(b'-y')(c'-z')}{a'b'c'} \quad N_3^e = \frac{x'y'(c'-z')}{a'b'c'}$$

$$N_4^e = \frac{(a'-x')y'(c'-z')}{a'b'c'} \quad N_5^e = \frac{(a'-x')(b'-y')z'}{a'b'c'} \quad N_6^e = \frac{x'(b'-y')z'}{a'b'c'}$$
$$N_7^e = \frac{x'y'z'}{a'b'c'} \quad N_8^e = \frac{(a'-x')y'z'}{a'b'c'} \tag{35}$$

and those in (24) are obtained by setting z' equal to zero. Here (x', y') denote the local coordinates associated with the e element and through a linear transformation they can be replaced by global coordinates. Substituting these into (18)-(20), (28) and (29), the resulting integrals can be evaluated analytically on the assumption of constant ϵ_r and μ_r within each element. The evaluation of the integrals in (25) and (26) is, however, more involved because of the kernel's singularity. To illustrate how these integrals could be evaluated let us consider one that has the generic form

$$p_{ij}^{ee'} = \iint_{S^e} N_i^e(x,y) \left[\iint_{S^{e'}} N_j^{e'}(x',y') G_0(\mathbf{R},\mathbf{R}') dS' \right] dS \tag{36}$$

If the eth and e'th elements are not adjacent, then mid-point integration could be used to evaluate $p_{ij}^{ee'}$ as

$$p_{ij}^{ee'} = N_i^e(x_c, y_c) N_j^{e'}(x_c', y_c') G_0(\mathbf{R}_c, \mathbf{R}_c') S^e S^{e'} \tag{37}$$

where the subscript c denotes the point at the center of the element. Otherwise, the eth and e'th elements could be subdivided into 3×3 small rectangles. Replacing the expansion functions N_i^e and $N_j^{e'}$ within each of nine rectangles with their mid-point values yields

$$p_{ij}^{ee'} = \sum_{m,n=1}^{3} \sum_{p,q=1}^{3} N_i^e(x_{mn}, y_{mn}) N_j^{e'}(x_{pq}', y_{pq}') g_{mnpq} \tag{38}$$

where

$$g_{mnpq} = \iint_{S_{mn}^e} \left[\iint_{S_{pq}^{e'}} G_0(\mathbf{R},\mathbf{R}') dS' \right] dS. \tag{39}$$

The integral g_{mnpq} can again be evaluated via mid-point integration provided (x, y) and (x', y') do not belong to the same rectangle, or share the same side. Otherwise, we rewrite g_{mnpq} as

$$g_{mnpq} = \frac{1}{4\pi} \iint_{S^e_{mn}} \left[\iint_{S^{e'}_{pq}} \left(\frac{e^{-jk_0|\mathbf{R}-\mathbf{R}'|}}{|\mathbf{R}-\mathbf{R}'|} - \frac{1}{|\mathbf{R}-\mathbf{R}'|} \right) dS' \right] dS + \frac{1}{4\pi} \iint_{S^e_{mn}} \left(\iint_{S^{e'}_{pq}} \frac{1}{|\mathbf{R}-\mathbf{R}'|} dS' \right) dS. \quad (40)$$

The first integral of these has a non-singular integrand and can therefore be evaluated numerically using a 2×2 Gaussian integration. The second integral has, of course, a singular integrand and must be evaluated analytically as described in [5].

IX. REFERENCES

[1] J. M. Jin and J. L. Volakis, "TE scattering by an inhomogeneously filled aperture in a thick conducting plane," *IEEE Trans. Antennas Propagat.*, accepted for publication.

[2] J. M. Jin and J. L. Volakis, "TM scattering by an inhomogeneously filled aperture in a thick conducting plane," *Proc. Inst. Elec. Eng., part H*, accepted for publication.

[3] S. K. Jeng, "Aperture admittance matrix by finite element method for scattering from a cavity-backed aperture," *1988 IEEE AP-S International Symposium Digest*, vol. 3, pp. 1134-1137, June 1988.

[4] S. W. Lee and H. Ling, "Data book for cavity RCS," (version 1), Electromagnetic Laboratory Technical Report SWL89-1, pp. 17-18, University of Illinois, January 1, 1989.

[5] K. Barkeshli and J. L. Volakis, "Scattering by an aperture formed by a rectangular cavity in a ground plane," Radiation Laboratory Technical Report 389757-1-T, The University of Michigan, December 1989.

[6] H. Ling, R. C. Chou, and S. W. Lee, "Shooting and bouncing rays: calculating the RCS of an arbitrarily shaped cavity," *IEEE Trans. Antennas Propagat.*, vol. AP-37, pp. 194-205, Feb. 1989.

[7] P. H. Pathak and R. J. Burkholder, "Modal, ray, and beam techniques for analyzing the EM scattering by open-ended waveguide cavities," *IEEE Trans. Antennas Propagat.*, vol. AP-37, pp. 635-647, May 1989.

[8] A. Taflove and K. R. Umashankar, "The finite-difference time-domain (FD-TD) method for electromagnetic scattering and interaction problems," *J. Electromagnetic Waves and Applications,* vol. 1, no. 4, pp. 363-387, 1987.

[9] O. C. Zienkiewicz, *The Finite Element Method,* 3rd ed. New York: McGraw-Hill, 1977.

[10] R. F. Harrington, *Time-Harmonic Electromagnetic Fields.* New York: McGraw-Hill, 1961.

[11] P. P. Silvester and R. L. Ferrari, *Finite Elements for Electrical Engineers.* Cambridge University Press, 1983.

[12] B. M. A. Rahman and J. B. Davies, "Penalty function improvement of waveguide solution by finite elements," *IEEE Trans. Microwave Theory Tech.*, vol. MTT-32, pp. 922-928, August 1984.

[13] J. M. Jin and V. V. Liepa, "Application of hybrid finite element method to electromagnetic scattering from coated cylinders," *IEEE Trans. Antennas Propagat.*, vol. AP-36, no. 1, pp. 50-54, Jan. 1988.

[14] A. George and J. Liu, *Computer Solutions of Large Sparse Positive Definite Systems.* Englewood Cliffs, NJ: Prentice-Hall, Inc., 1981.

[15] J. M. Jin and V. V. Liepa, "A note on hybrid finite element method for solving scattering problems," *IEEE Trans. Antennas Propagat.*, vol. AP-36, no. 10, pp. 1486-1490, Oct. 1988.

[16] J. R. Mautz and R. F. Harrington, "Electromagnetic transmission through a rectangular aperture in a perfectly conducting plane," Scientific Report No. 10, Contract F19628-73-C-0047 with Air Force Cambridge Research Laboratories, Hanscom A.F.B., Mass., Feb. 1976.

[17] G. Mur and A. T. de Hoop, "A finite-element method for computing three-dimensional electromagnetic fields in inhomogeneous media," *IEEE Trans. Magnetics*, vol. MAG-21, pp. 2188-2191, Nov. 1985.

[18] J. Van Bladel, "Field singularities at metal-dielectric wedges," *IEEE Trans. Antennas Propagat.*, vol. AP-33, no. 4, pp. 450-455, April 1985.

[19] J. P. Webb, "Finite element analysis of dispersion in waveguides with sharp metal edges," *IEEE Trans. Microwave Theory Tech.*, vol. MTT-36, pp. 1819-1824, Dec. 1988.

FIGURE CAPTIONS

Fig. 1 Geometry of a cavity-backed aperture in a ground plane.

Fig. 2 Aperture field distribution (E_y) at the center of a narrow crack. $b = 0.05\lambda$, $c = 0.25\lambda$, $\epsilon_r = 1.0$, $\mu_r = 1.0$, normal incidence. (a) $a = 0.5\lambda$. (b) $a = 1.0\lambda$. (c) $a = 1.5\lambda$. (d) $a = 2.0\lambda$.

Fig. 3 Backscatter RCS patterns for an empty cavity versus incidence angle. $a = 0.7\lambda$, $b = 0.1\lambda$, $c = 1.73\lambda$, $\theta = 40^o$. Solid and dashed lines represent the solution of this method; circles and squares represent the moment method/modal solution [5]. (a) $\alpha = 90^o$ ($\mathbf{E} = \hat{\phi}E_\phi$). (b) $\alpha = 0^o$ ($\mathbf{E} = \hat{\theta}E_\theta$).

Fig. 4 Backscatter RCS for an empty cavity as a function of cavity depth. $a = 0.7\lambda$, $b = 0.1\lambda$, $\theta = 40^o$.

Fig. 5 Backscatter RCS patterns for a material-filled cavity versus incidence angle. $a = 1.0\lambda$, $b = 0.25\lambda$, $c = 0.25\lambda$, $\epsilon_r = 7.0 - j0.5$, $\mu_r = 1.8 - j0.1$. Solid and dashed lines represent the solution of this method; circles and squares represent the moment method/modal solution [5]. (a) $\phi = 90^o$. (b) $\phi = 0^o$.

Fig. 6 Backscatter RCS patterns for a multilayer material-filled cavity versus incidence angle. $a = 1.0\lambda$, $b = 0.25\lambda$, $c = 0.25\lambda$. Top layer: $\epsilon_r = 7.0 - j0.5$, $\mu_r = 1.8 - j0.1$, t (thickness)$= 0.0625\lambda$; middle layer: $\epsilon_r = 3.0 - j0.05$, $\mu_r = 2.0$, $t = 0.125\lambda$; bottom layer: $\epsilon_r = 5.0 - j0.03$, $\mu_r = 1.0$, $t = 0.0625\lambda$. Solid and dashed lines represent the solution of this method; circles and squares represent the two-dimensional solution [1], [2]. (a) $\phi = 90^o$. (b) $\phi = 0^o$.

Fig. 7 Geometry of a rectangular brick.

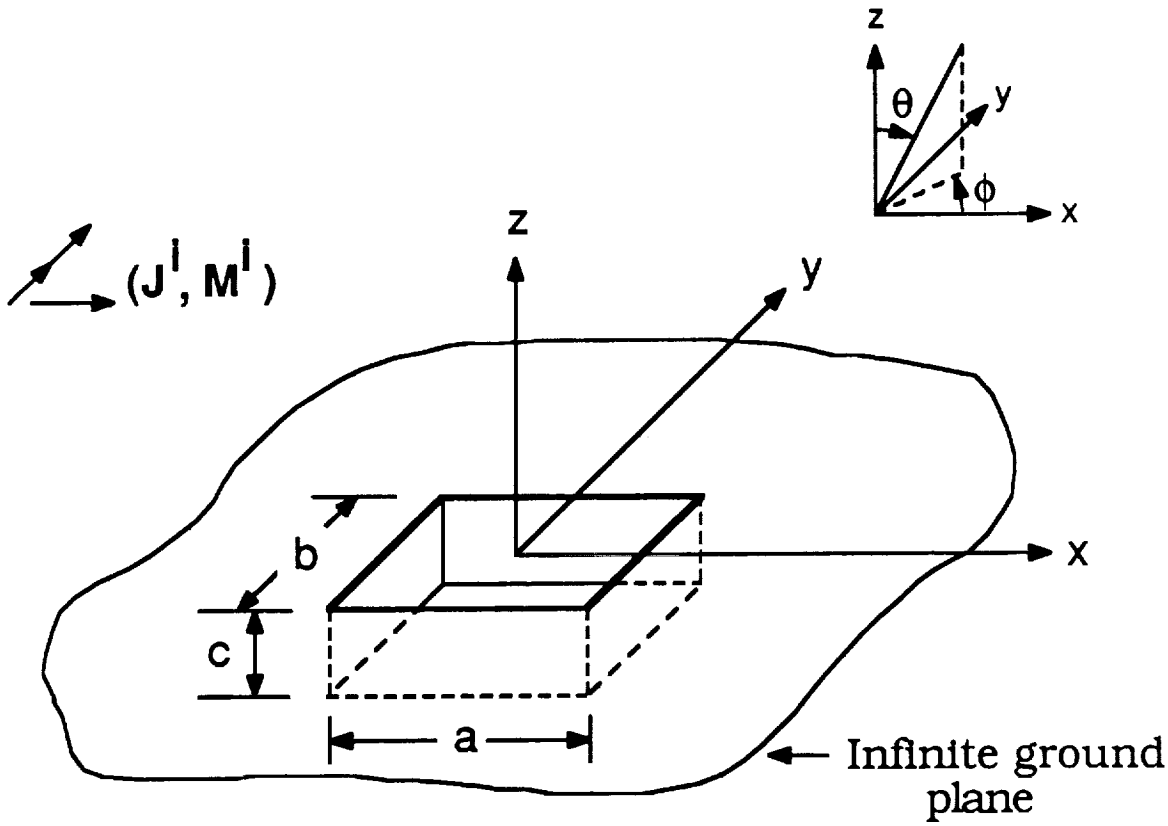

Fig. 1

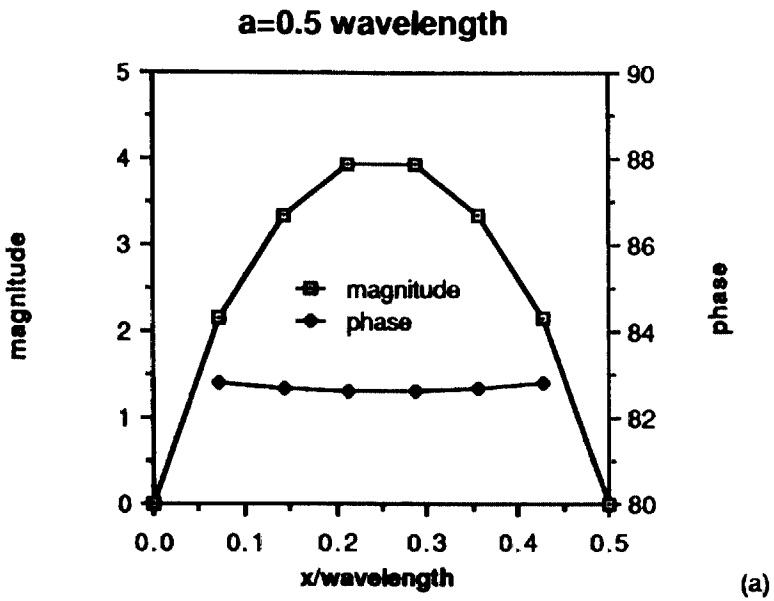
a=0.5 wavelength
magnitude
phase
x/wavelength
magnitude
phase
0
1
2
3
4
5
80
82
84
86
88
90
0.0
0.1
0.2
0.3
0.4
0.5

(a)

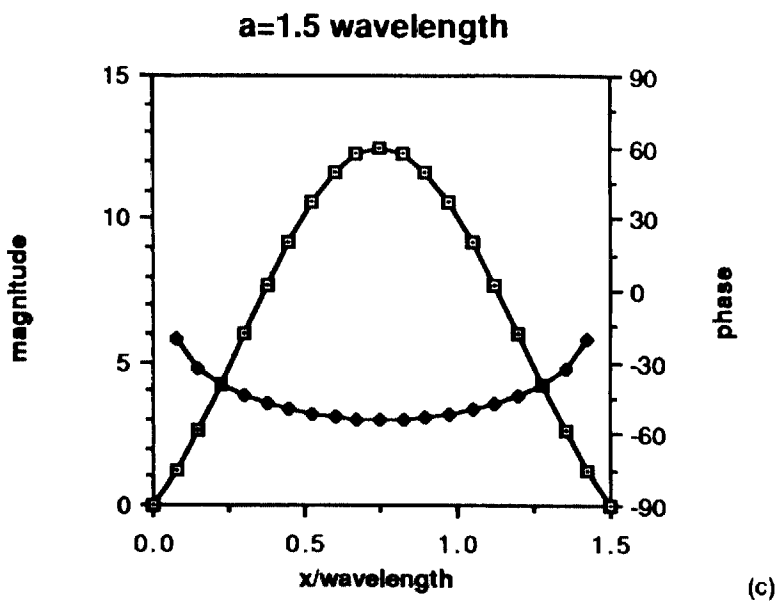
a=1.5 wavelength
magnitude
phase
x/wavelength
0
5
10
15
-90
-60
-30
0
30
60
90
0.0
0.5
1.0
1.5

(c)

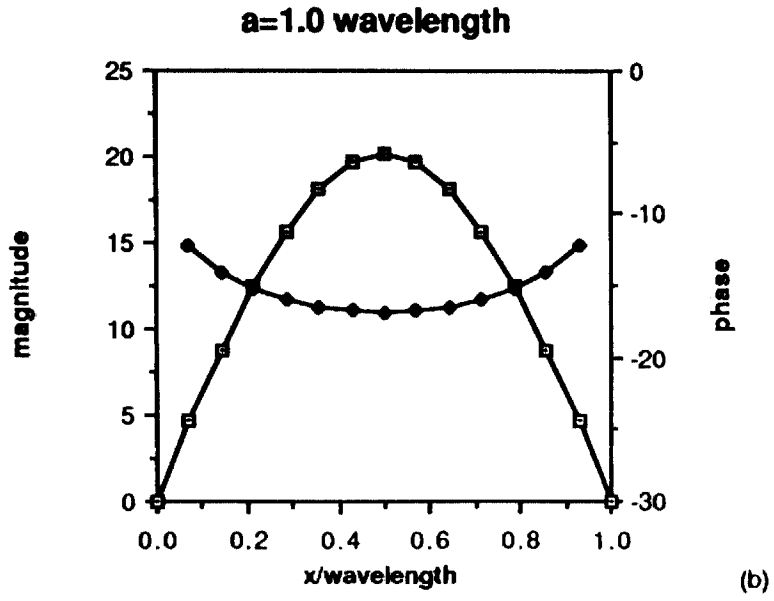
a=1.0 wavelength
magnitude
phase
x/wavelength
0
5
10
15
20
25
-30
-20
-10
0
0.0
0.2
0.4
0.6
0.8
1.0

(b)

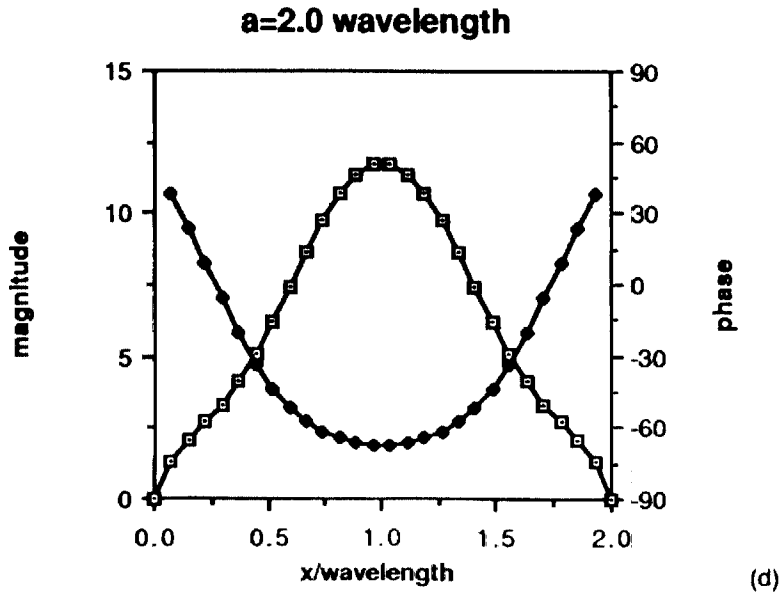
a=2.0 wavelength
magnitude
phase
x/wavelength
0
5
10
15
-90
-60
-30
0
30
60
90
0.0
0.5
1.0
1.5
2.0

(d)

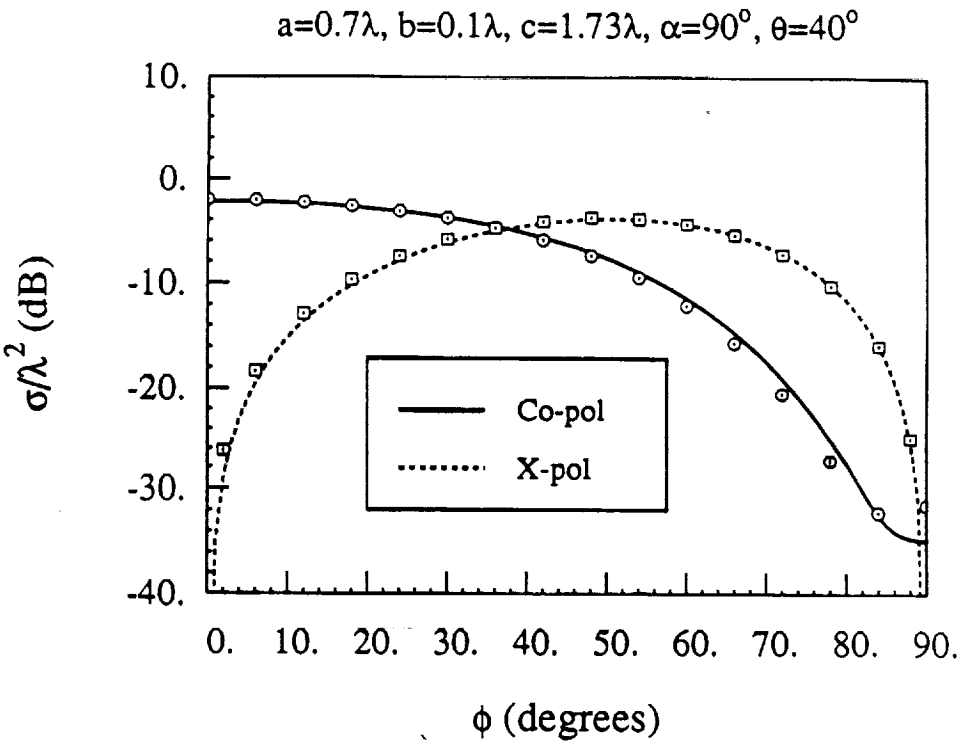
a=0.7λ, b=0.1λ, c=1.73λ, α=90°, θ=40°
10.
0.
-10.
-20.
-30.
-40.
σ/λ² (dB)
Co-pol
X-pol
0. 10. 20. 30. 40. 50. 60. 70. 80. 90.
φ (degrees)

(a)

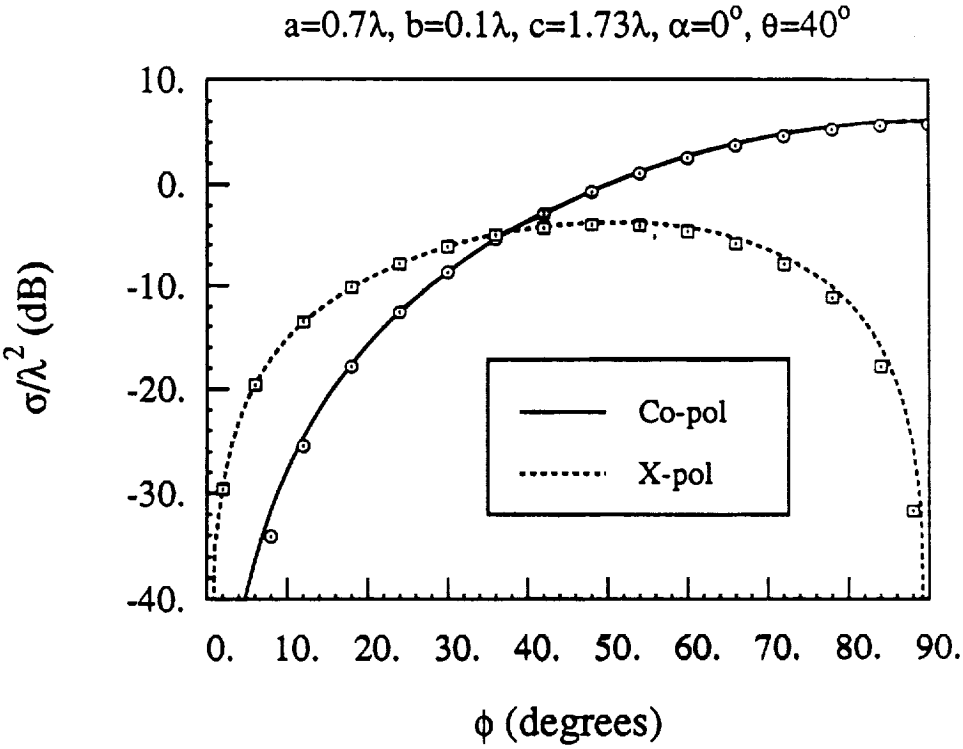
a=0.7λ, b=0.1λ, c=1.73λ, α=0°, θ=40°
10.
0.
-10.
-20.
-30.
-40.
σ/λ² (dB)
Co-pol
X-pol
0. 10. 20. 30. 40. 50. 60. 70. 80. 90.
φ (degrees)

(b)

Fig. 3

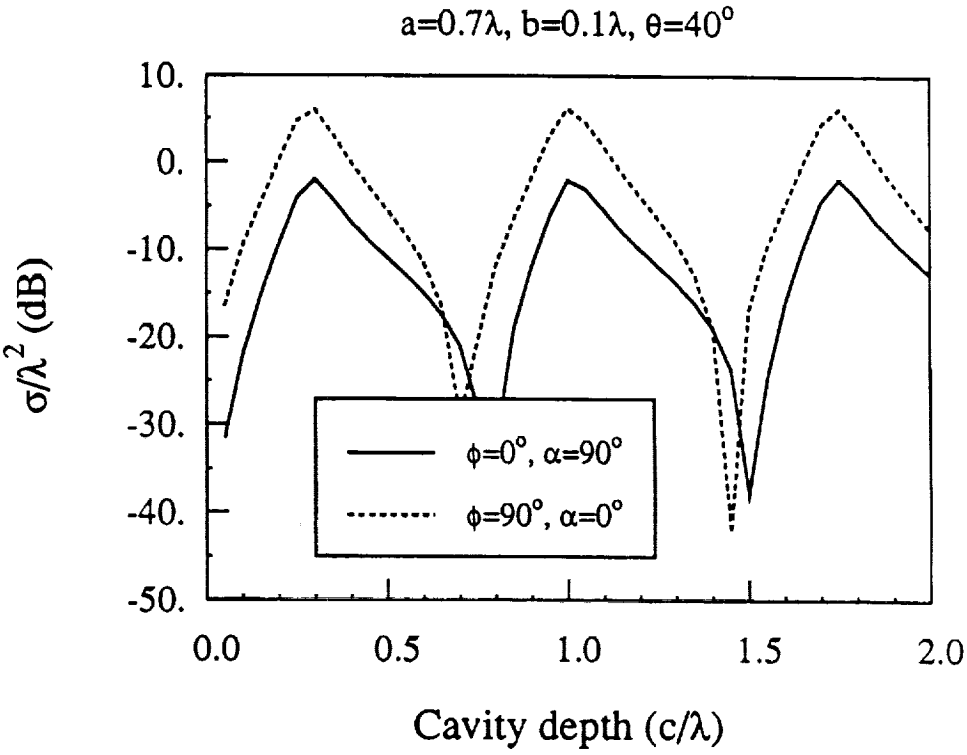
a=0.7λ, b=0.1λ, θ=40°
10.
0.
-10.
-20.
-30.
-40.
-50.
σ/λ² (dB)
0.0
0.5
1.0
1.5
2.0
Cavity depth (c/λ)
ϕ=0°, α=90°
ϕ=90°, α=0°

Fig. 4

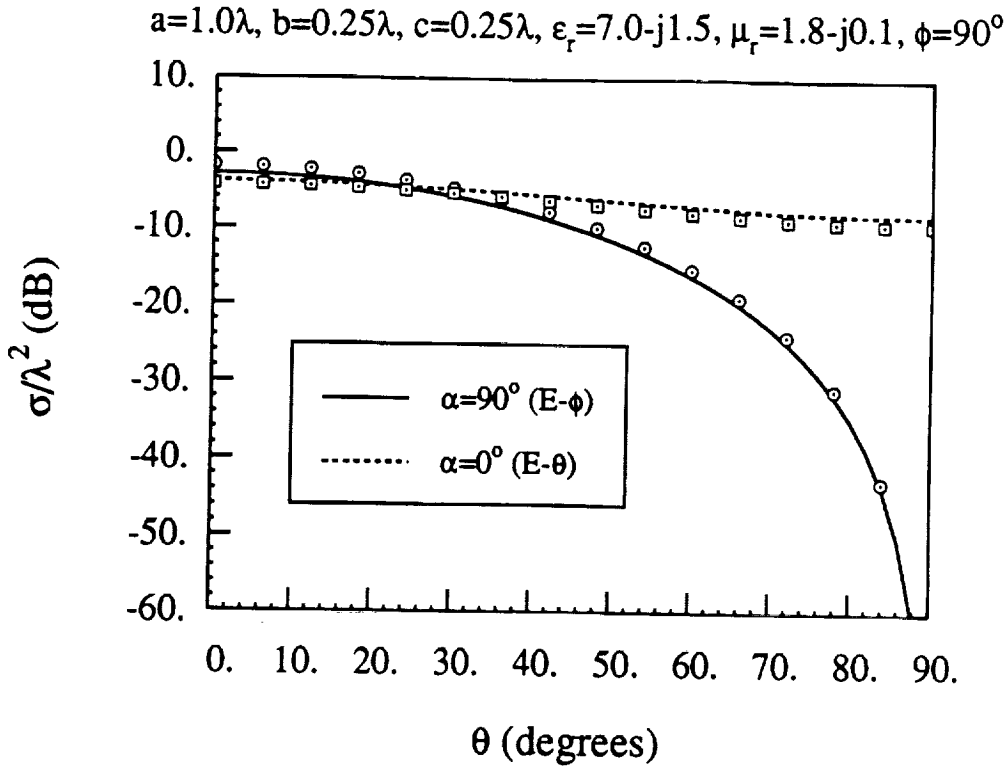
a=1.0λ, b=0.25λ, c=0.25λ, εr=7.0-j1.5, μr=1.8-j0.1, ϕ=90°
10.
0.
-10.
-20.
-30.
-40.
-50.
-60.
σ/λ² (dB)
α=90° (E-ϕ)
α=0° (E-θ)
0. 10. 20. 30. 40. 50. 60. 70. 80. 90.
θ (degrees)

(a)

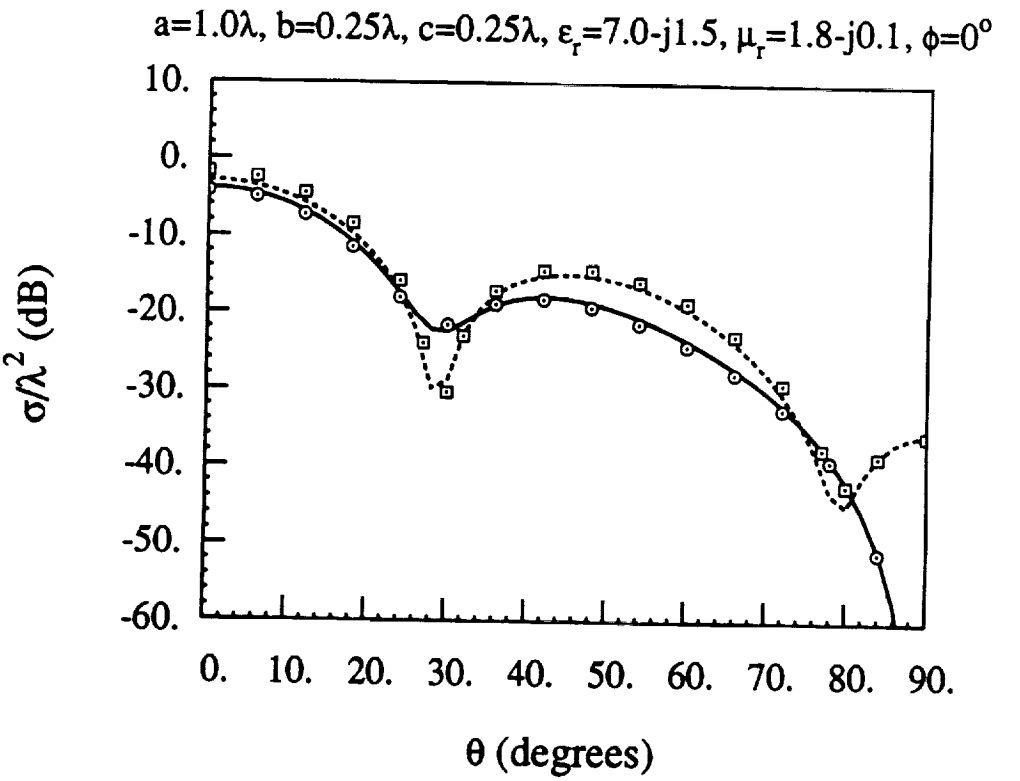
a=1.0λ, b=0.25λ, c=0.25λ, εr=7.0-j1.5, μr=1.8-j0.1, ϕ=0°
10.
0.
-10.
-20.
-30.
-40.
-50.
-60.
σ/λ² (dB)
0. 10. 20. 30. 40. 50. 60. 70. 80. 90.
θ (degrees)

(b)

Fig. 5

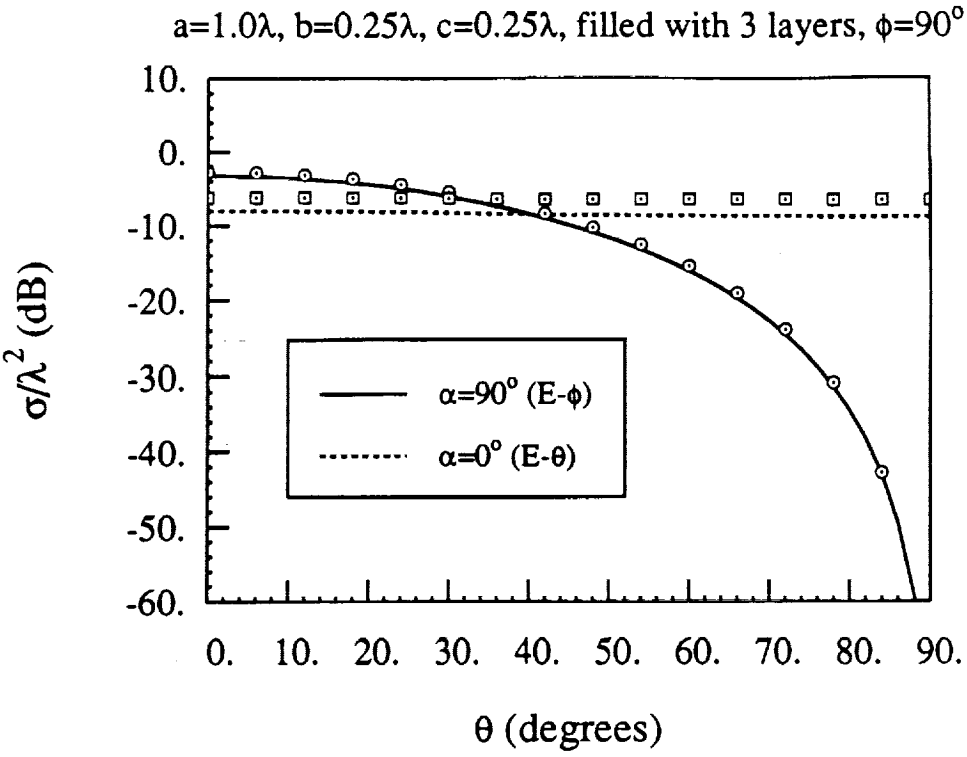
a=1.0λ, b=0.25λ, c=0.25λ, filled with 3 layers, ϕ=90°
10.
0.
-10.
-20.
-30.
-40.
-50.
-60.
σ/λ² (dB)
α=90° (E-ϕ)
α=0° (E-θ)
0. 10. 20. 30. 40. 50. 60. 70. 80. 90.
θ (degrees)

(a)

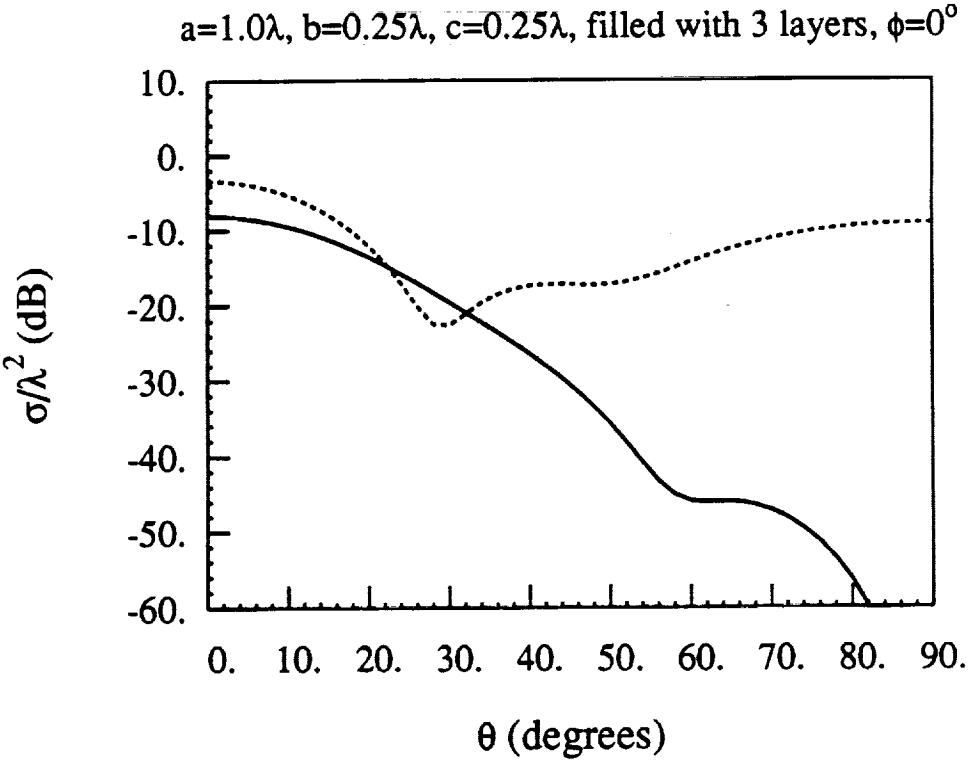
a=1.0λ, b=0.25λ, c=0.25λ, filled with 3 layers, ϕ=0°
10.
0.
-10.
-20.
-30.
-40.
-50.
-60.
σ/λ² (dB)
0. 10. 20. 30. 40. 50. 60. 70. 80. 90.
θ (degrees)

(b)

Fig. 6

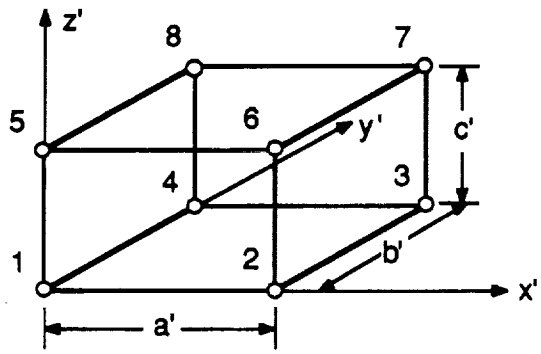

Fig. 7